Pergamon PII: S0038–092X(99)00044–4
www.elsevier.com/locate/solener
Solar Energy Vol. 68, No. 1, pp. 91–107, 2000

0038-092X/00/$ - see front matter

EFFECTS OF BURNING OF BIOMASS ON SATELLITE ESTIMATIONS OF SOLAR IRRADIATION IN BRAZIL

E. B. PEREIRA*,†, F. R. MARTINS*, S. L. ABREU**, P. COUTO**, R. STUHLMANN*** and S. COLLE**

*INPE, C. Postal 515, S.J. Campos, SP-12201-970, Brazil
**UFSC/EMC/Labsolar, C. Postal 476, Florianópolis, SC-88040-900, Brazil
***GKSS Forschungszentrum, D-21502 Geesthacht, Germany

Received 14 October 1998; revised version accepted 13 April 1999

Communicated by AMOS ZEMEL

Abstract—Atmospheric combustion products from forest fires in the Brazilian Amazon and 'Cerrado' regions during the dry season (July–October) induce systematic deviations on the routine satellite techniques for the assessment of solar energy resource information. This study, based on clear-sky days, has shown model overestimations of the incoming solar radiation as high as 44%. On the average, clear-sky model overestimation was four times larger than that found for clear-sky days in regions outside the biomass-burning season. A positive correlation between the combustion products of black carbon, total aerosols, CO, N_2O, CH_4, and the number of fire spots counted by the AVHRR sensor from the NOAA series satellites suggests a possible mechanism for the parameterization of these effects on the radiation transfer methods.

1. INTRODUCTION

The long-range policy for the use of solar energy in countries of the tropical belt must take into account some local environmental characteristics that are only poorly assessed so far. The intensive cloud convection which is associated with the inter-tropical convergence zone (ITCZ); and the manmade changes in the biosphere–atmosphere interaction, triggered by deforestation and land clearings are among the most important factors. The first factor hinders reliable use of satellite data for solar energy resource budget evaluation due to inadequate parameterization of clouds by the current radiation transfer models. Although parameterization of clouds can be very sophisticated in radiative transfer models (even 3-D effects), the necessary input from operational satellite data may still not be able to be obtained to perform the calculations. The second affects the solar radiation budget in the atmosphere due to combustion by products injected into the atmosphere by the widely used practice of land clearings for farming and cattle growth. The magnitude of this effect, however, remains a controversial issue particularly with regard to the aerosols.

Although it has been recognized that aerosols exert a climatic effect on the atmosphere by producing net cooling (Charlson *et al*., 1992; Coakley *et al*., 1993), less attention has been devoted to this study from the point of view of the evaluation of the solar energy resource information. Whitlock and Tarplay (1996) have previously reported the role of biomass combustion products on the transparency of the atmosphere. They have shown the influence of forest fire occurrence in Africa between 1986 and 1987 on Pinker's algorithm to infer solar irradiation at the surface. Model overestimation of as much as 120 $W\,m^{-2}$ has been reported and linked to forest fires located south of the ground radiation sites. Using recent values of biomass burning, Anderson *et al*. (1996) calculated that diluted smoke from biomass burning plumes produce an average tenfold enhancement in optical depth over continental regions which translates into a -25 $W\,m^{-2}$ net radiative forcing during clear-sky conditions.

According to up-to-date (1998) information from the Brazilian National Institute for Space Research, INPE *(http://www.inpe.br)*, current estimation for deforestation rate in the Amazon region[1] is 18 000 km^2/year. The resulting total

†Author to whom correspondence should be addressed. Tel.: +55-12-345-6741; fax: +55-12-345-6810; e-mail: enio@dge.inpe.br

[1]The legal Brazilian Amazon region, also known as the North regional division, comprises the states of Amazonas, Pará, Tocantins, Roraima, Amapá, Acre and Rondônia.

emission of particulate matter from this source has been estimated at some 10^{14} g of particulate matter to the atmosphere per year (Crutzen and Andreae, 1990; Ward *et al.*, 1992). Black carbon accounts for about 10% of this total anthropogenic release, and is of major concern for its distinctive low single scattering albedo. The assessment of this emission in the solar radiation budget in the atmosphere is of major scientific concern (Kirchhoff, 1996).

This paper assesses the effects of the biomass burning on satellite estimations of the surface solar radiation in Brazil during the dry season (July–October) using the BRASIL-SR model.

2. THE BRASIL-SR RADIATIVE TRANSFER MODEL

2.1. Description of the model

In order to evaluate radiative forcing at the surface by the biomass combustion products in Brazil, the BRASIL-SR model was used in conjunction with ground radiation data from selected sites. This radiation model was originally developed in Germany (GKSS, Geesthacht) by Möser and Raschke (1983) and later adapted and improved to operate in Brazil by a joint collaboration between the Federal University of Santa Catarina (UFSC) and the Brazilian National Institute for Space Research (INPE). It is a physical model that employs the visible narrow-band response of a geostationary satellite to estimate the broadband solar radiation at the surface. Since both the reflected radiation at the top of the atmosphere and the surface incident solar radiation are mainly dependent on the cloud optical thickness, the model assumes that clouds are the first-order factor modulating the solar radiation field in the atmosphere. The upward solar density flux at the top of the atmosphere $F_{\uparrow}$ increases with the increase of cloud optical thickness δ and the downward surface radiation flux $F_{\downarrow}$decreases. Thus, for clear-sky conditions the upward flux at the top of the atmosphere reaches its minimum, which is primarily a function of the atmospheric transmittance and of the surface albedo. For fully overcast conditions, when the cloud optical thickness reaches its maximum, the upward flux at the top of the atmosphere is at its maximum owing to the cloud albedo. These two extreme sky conditions can be modeled with a satisfactory degree of confidence. However, the same cannot be said for sky conditions lying in between these two extremes.

The parameterization of the all-sky transmittance is a difficult task due to its highly stochastic nature. Nonetheless, it can be made by assuming that the upward flux $F_{\uparrow}$ may be split into two independent contributions: the first component corresponds to cloud-free sky conditions $F_{\text{clear}\uparrow} = f(\tau_a,\ F_0,\ \theta_z,\ \rho_s)$; and the second to overcast conditions $F_{\text{cloud}\uparrow} = g(F_0,\ \theta_z,\ \delta)$. The τ_a is the atmospheric transmittance, θ_z is the solar zenith angle, F_0 is the incoming solar radiation flux at the top of the atmosphere, δ is the cloud optical thickness, and ρ_s is the surface albedo. These components can be estimated on the basis of a known set of input atmospheric data. The stochastic nature of the all-sky solar radiation field is included in the model by defining a fractional or effective cloud cover, n_{eff} where the $F_{\uparrow}$ is linearly distributed between these two extreme atmospheric conditions, $F_{\text{clear}\uparrow}$and $F_{\text{cloud}\uparrow}$:

$$F_{\uparrow} \approx (1 - n_{\text{eff}})F_{\text{clear}\uparrow} + n_{\text{eff}}F_{\text{cloud}\uparrow} \tag{1}$$

Thus, it follows by isolating n_{eff}:

$$n_{\text{eff}} \approx (F_{\uparrow} - F_{\text{clear}\uparrow})/(F_{\text{cloud}\uparrow} - F_{\text{clear}\uparrow}) \tag{2}$$

Assuming that the broadband defined n_{eff} can be adequately represented in terms of the short band readings from the satellite sensor L, we can rewrite Eq. (2) as:

$$n_{\text{eff}} \approx (L - L_{\text{min}})/(L_{\text{max}} - L_{\text{min}}) \tag{3}$$

where the min and max subscripts stand, respectively, for maximum and minimum satellite readings. Note that the left term of Eq. (3) is a non-dimensional relative quantity and thus, the estimation of n_{eff} can be made directly in terms of the digital counts obtained from the satellite sensor with no need for sensor calibration.

The major assumption made by this model is that there is a negative correlation between the sky transmittance and the fractional cloud amount measured by n_{eff}. This can be represented by a simple linear function of the type:

$$n_{\text{eff}} = 1 - \frac{\tau - \tau_{\text{cloud}}}{\tau_{\text{clear}} - \tau_{\text{cloud}}} \tag{4}$$

By rewriting Eq. (4) and keeping in mind that F_0 is the extraterrestrial downward radiation flux, we can finally arrive with the expression for the downward solar radiation flux at surface $F_{\downarrow}$:

$$F_{\downarrow} = [n_{\text{eff}}\tau_{\text{cloud}} + (1 - n_{\text{eff}})\tau_{\text{clear}}]F_0 \tag{5}$$

Therefore, in order to obtain the surface irradiance $F_{\downarrow}$ we need the satellite information on fractional cloud cover n_{eff} and on the two boundary values for the sky transmittance τ_{clear} and τ_{cloud}. These

two boundary values are estimated by using the two-stream radiative transfer scheme developed by Schmetz (1984). This one-dimensional radiative transfer scheme accounts for absorption and scattering by gases and aerosols assuming realistic atmospheres. Input parameters are the single scattering albedo ϖ, the optical depth δ, and the asymmetry parameter of the phase function g, as described by the coupled differential equations for the two-stream method (Lenoble, 1985). Furthermore, the two-stream scheme is applied for a total of 135 radiation wavelength intervals in the shortwave solar spectral band (0.3–3 μm).

Several types of model atmospheric profiles (sub-arctic and mid-latitude summer and winter, and tropical) are used, based on ground data for temperature, relative humidity, and horizontal visibility. The scheme simulates an inhomogeneous atmosphere by dividing each profile into 31 pressure levels which define 30 homogeneous atmospheric layers up to the top of the atmosphere, for which temperature, dry air density, ozone and carbon dioxide concentrations, and the ϖ and g parameters are prescribed. In addition, the water vapor and aerosol loads are estimated by using simple approximations. The upward ($F_{\uparrow}$) and downward ($F_{\downarrow}$) diffusive fluxes obtained by solving the coupled two-stream differential equations are applied for each layer subjected to the boundary conditions below:

$$F_{i\uparrow}(\delta = \Delta\delta_i) = F_{i+1\uparrow}(\delta = 0)$$
$$F_{i\downarrow}(\delta = \Delta\delta_i) = F_{i+1\downarrow}(\delta = 0) \quad (6)$$

Where F_i is the diffusive flux applied to the ith (counted downwards) atmospheric layer. Boundary conditions established at the top of the atmosphere and at the surface provide the linear equation system which can be solved to get the resulting diffusive radiation density fluxes at surface and, consequently, the two boundary values τ_{clear} and τ_{cloud}.

The parameterization of the aerosol light scattering and absorption is made by employing the very simple Angström empirical formulation (Iqbal, 1983) which states that the direct transmittance for solar beam radiation can be approached by:

$$\tau_{a\lambda} = \exp(-\beta\lambda^{-\alpha} m_{\text{a}}) \quad (7)$$

Where β and α are coefficients, λ is the wavelength, and m_a is the optical air mass. The input parameter for the model is $\beta\lambda^{-\alpha}$ in 37 radiation wavelength intervals of the shortwave solar spectral band and three different altitude ranges: below 2 km, between 2 km and 10 km, and above 10 km.

The optical air mass was estimated using aerosol profiles described by McClatchey and Selby (1972) for 0–50 km altitudes. The first 5 km of the profile were corrected in terms of the empirical horizontal visibility ranges, also called *meteorological ranges* (*VIS*). This procedure sets the optical air mass at sea level, and an exponential correction was applied when ground station is above sea level.

This procedure is sufficient to parameterize the aerosol effects in most cases, as will be seen below. Nevertheless, this simple approach cannot cope with some unique atmospheric environments such as large urban areas and regions where intensive burning of biomass is practiced, like in the northern and central regions of Brazil and in central Africa during the dry season.

2.2. Satellite data acquisition and processing

The algorithm employs digital data from GOES-8 satellite sensor in the visible channel (0.52–0.72 μm). This satellite, which is also known as GOES-EAST, is located at about 75°W at the equator. The Brazilian National Institute Space Research collects raw satellite data at 12.00 GMT, 15.00 GMT and 18.00 GMT, through its division of Environmental Satellites-INPE/DSA in Cachoeira Paulista, Brazil at an 8 km×4.6 km horizontal ground resolution at satellite nadir.

The raw data are recorded onto CD-ROM for later processing after necessary editing and corrections to remove or repair bad data. The input data for the model are the n_{eff} values, which embody the cloud variability. Eq. (3) calculates n_{eff} for each pixel (picture element of the digital image) from the raw satellite data. Figs. 1(a) and 1(b) shows the block diagram of the BRAZIL-SR.

The model also requires information on the other atmospheric constituents, ground albedo, and altitude in order to generate the atmospheric profiles for the two-stream radiative transfer calculation. Since clouds are the most important factor of modulation of the radiation field, other atmospheric constituents are only of secondary order and are assumed to be sufficiently described by their monthly mean climatology. Thus, the ground temperature and relative humidity are obtained from the 30-year climatic tables from the Brazilian National Institute of Meteorology (INMET, 1992). Topography is obtained from EROS Data Center–Distributed Active Archive Center (EDC–DAAC), USA, at 30″ horizontal ground resolution and 100 m vertical resolution.

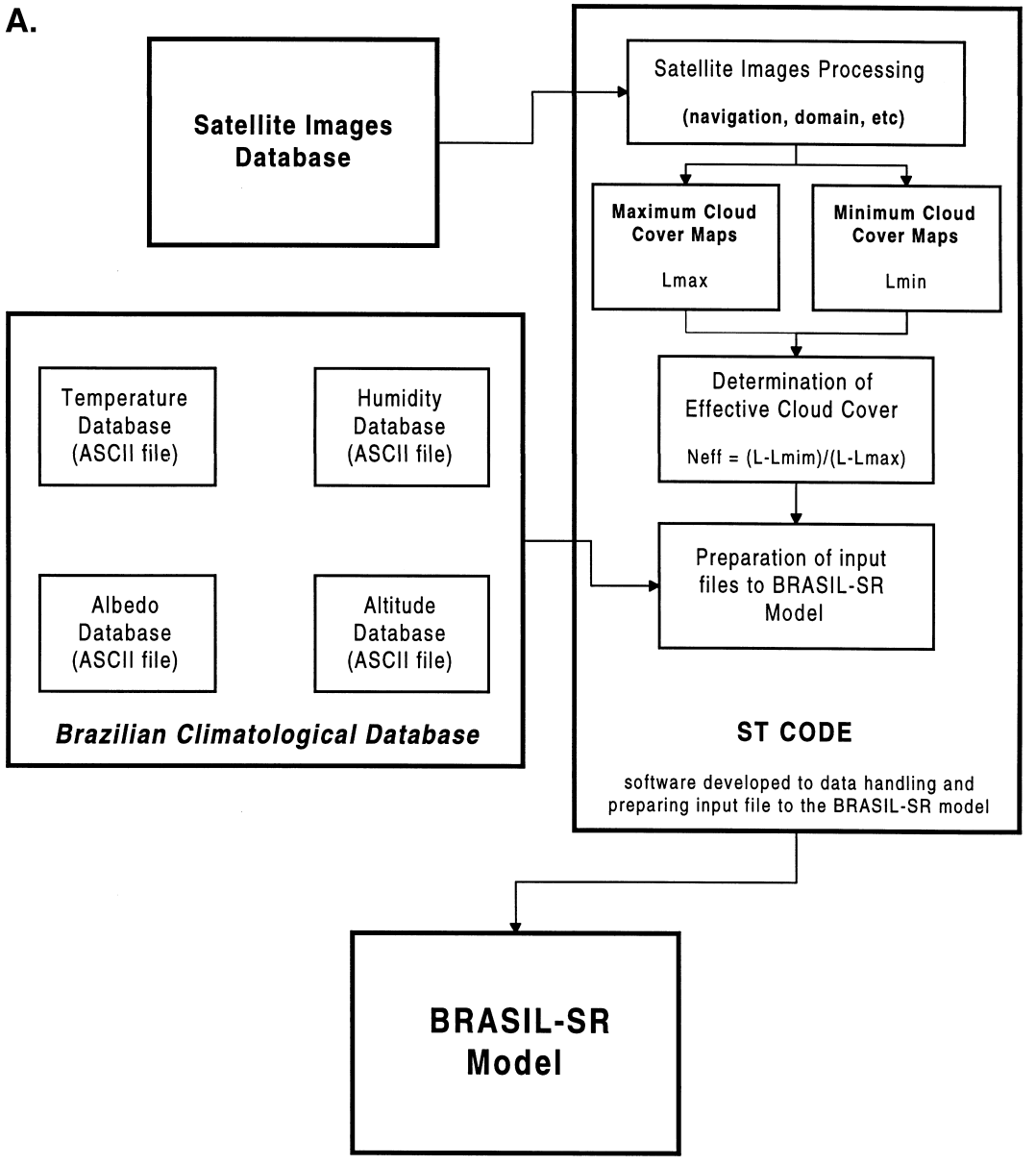

Fig. 1. Block diagram for the input data and model parameters for the BRASIL-SR (a) and block diagram of the model BRASIL-SR radiation transfer model program (b).

The albedo is obtained from the DAAC–Langley ISCCP data product. All these input data are reduced to the same horizontal ground resolution of $0.5° \times 0.5°$ by interpolation techniques, which defines the final pixel size for the model computation.

3. BURNING OF BIOMASS

One practical way to estimate the intensity of the burning activities of biomass in large continental areas such as Brazil is by using the satellite technique described by Pereira and Setzer (1993). Fire spots are routinely detected by the AVHRR thermal channel from satellites of the NOAA series. This technique uses the thermal (channel 3) region of the solar spectrum which comprises the 3.55–3.93 μm range, to count the number of pixels that are associated with a ground fire. The method does not quantitatively derive the area where fires occur, nevertheless, independent measurements have shown that fires as small as 30 m in length can provide sufficient energy in the thermal band to saturate a pixel in the gray scale, and can be counted as a single fire spot. The size of the pixel at the nadir is about 1 km^2.

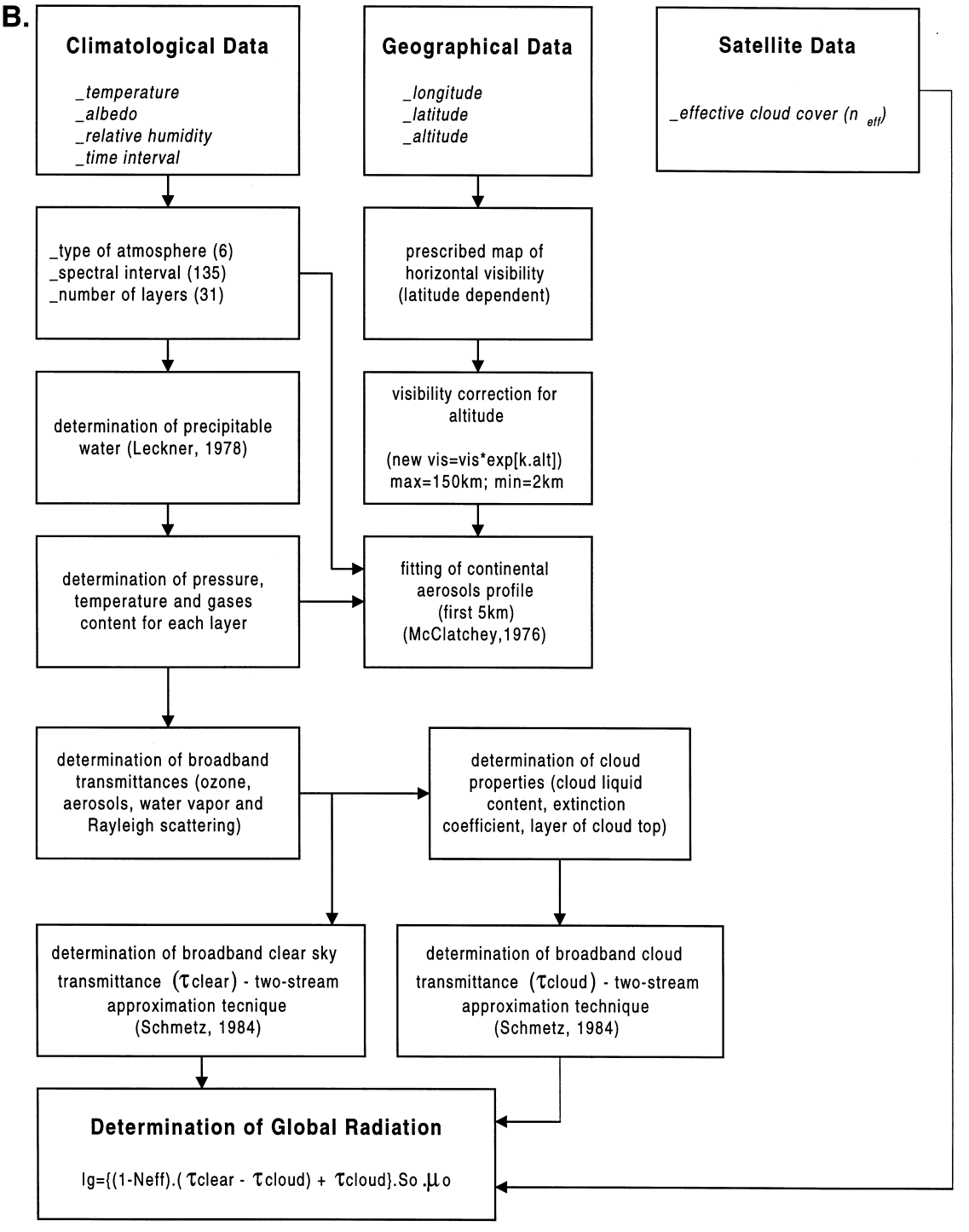

Fig. 1. (*continued*)

Thus, in spite of the non-linearity and qualitative characteristics of this method, one can assume that the number of fire spots is proportional to the area hit by the fires.

The Division of Satellite Products of INPE, located in Cachoeira Paulista-São Paulo, systematically collects the raw satellite images on a daily basis during the period June–November, which comprises the period of peak fire activity. The images are automatically processed and the integrated results on fire spots are made available to the public at the INPE's home page site: *http://www.dsa.inpe.br*. Fig. 2 shows the monthly relative frequency of fire spots for the available

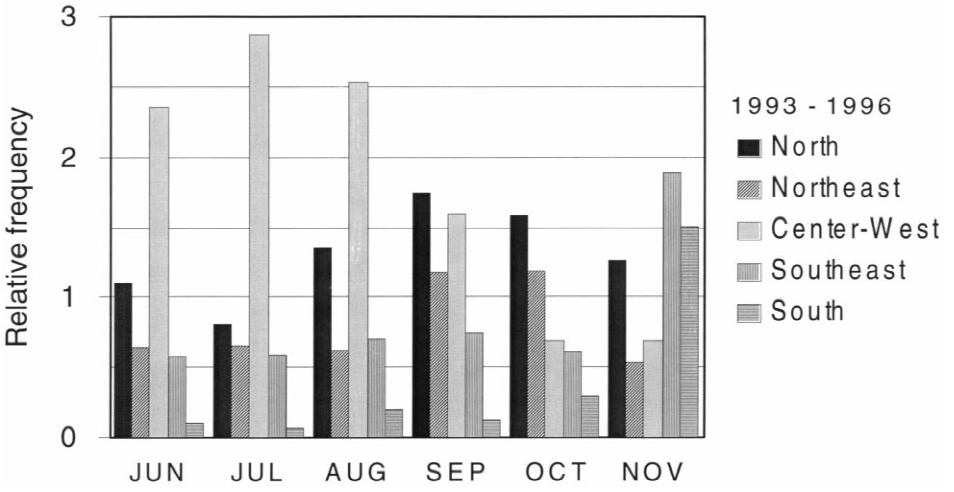

Fig. 2. Relative frequency of the number of fire spots detected by the AHVRR satellite sensor as a function of the month for the five main climatic regions of Brazil.

period. Fire spot data are available for both NOAA 12 and 14 satellites. Since each satellite views a different scene at a different time of the day, it was necessary to normalize the data in such a way as only the relative increments of fire spots were shown. This was made by dividing the monthly average fire spots by the corresponding total number of fire spots (all five regions). By using this procedure, it was possible to combine data sets from different satellites into a larger one, which resulted in significant improvements.

The peak of the burning season in the northern region, which includes the Amazon forest area, occurs between September and October, while for the Central[2] region, in the 'Cerrados' plateau area of Brazil, it is in June–July. Fires in other regions are negligible compared to these two regions. Furthermore, the emission factors of total particulate carbon, aerosols, and gaseous combustion products by flaming and smoldering forests are generally larger than for grass and 'Cerrados' (Ferek *et al.*, 1997).

For comparison, Fig. 3 presents the geographic distribution of fire spots counted in the whole of Brazil for the months of June 1996 and September 1996, respectively, at the beginning and at the peak of the fire season. In September fire spots spread out throughout a large area in Brazil with some 'hot spots' in the state of Tocantins where intensive clearing activities are concentrated. The distribution of fires is more strongly concentrated around the Amazon forest border, progressively spreading out towards the South–Southeast sector of the country. In contrast, we observe a meager density of fires during the month of June, which marks the onset of the burning season in this country. Although the fire spot density is sparse in June for most of the country, constant biomass burning activities are observed in the state of São Paulo, linked to the harvesting of sugarcane for the local alcohol industry.

Fig. 3 were derived from nighttime overpasses of NOAA-12 over Brazil. Comparison with afternoon overpasses of NOAA-14 (not presented) show a much smaller number of fire spot counts. This was explained by the fact that fires are usually ignited just after noontime. At night, some of these fires have already died or are in a smoldering phase. Data set of the NOAA-14 satellite were not complete due to the influence of the sun glint during part of the year, thus were not qualified for this study.

Fig. 4 shows the plot of the annual mean daily global horizontal surface solar radiation between 1995 and 1998 estimated by the BRAZIL-SR model. The maximum irradiation takes place in the states of the Northeast, along a band that stretches NE–SW from the northern part of the state of Bahia through the state of Ceará, and in the northern border of the state of Roraima, with daily averages peaking above 22 $MJ\,m^{-2}$. The Northeast region is under the influence of a tropical high pressure linked to the South Atlantic tropical anticyclone during the whole year which confer this semi-arid region a stable regime of high surface solar irradiation. The lowest surface irradiation is observed in the eastern part of the states of Paraná and Santa Catarina, with daily

[2]The Central divisional region of Brazil comprises the states of Mato Grosso, Goiás and Mato Grosso do Sul.

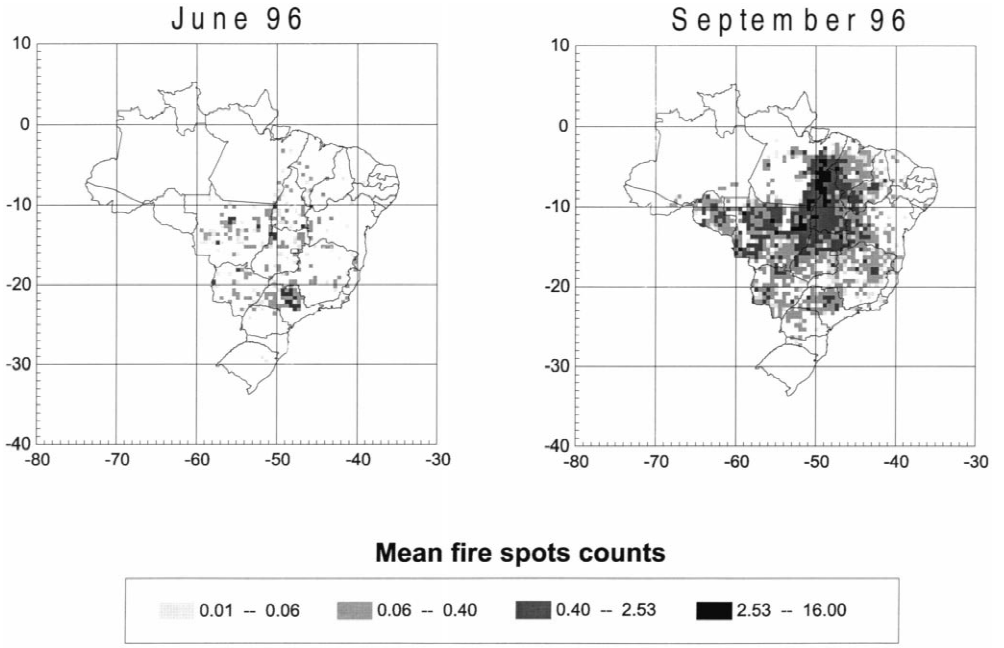

Fig. 3. Geographical distribution of the total number of fire spots counted during the months of June and September of 1996. Data were calculated by using the NOAA-12 AVHRR thermal sensor.

averages of 15 MJ m^{-2}. Comparing Figs. 3 and 4 one can see that areas with maximum solar irradiation in Brazil are also more or less coincident with the areas were biomass-burning activities occur. Thus the assessment of the effects of the biomass combustion products on the model estimation is an important issue for this region.

Wintertime in the Southern Hemisphere starts in July and ends in September. During this period most of the country is under the influence of a dry stable tropical maritime air mass. In the Amazon and in the central plateau regions this period is also known as the dry season for its relatively cloudless sky, low rain activity and low relative humidity. The surface solar irradiation is the highest and the variability, measured by the standard deviation divided by the mean of the daily solar radiation at each pixel of the image, is the lowest of the year. This can be seen in Fig. 5, which shows the global horizontal surface irradiance and its variability as a function of the month for northern and central Brazil. Note by comparing Figs. 2 and 5 that the periods of maximum occurrences of fire events are coincident with periods of more stable regime of solar irradiation. The decline in rain activity and the more stable regime are the reasons why the farmers choose this time of the year for the process of clearing the forest for pastureland and/or agriculture purposes. Large trees are cut and let dry. Fires are induced only when rain activity is a minimum for a long period, which occurs during the dry season.

4. FIRE PRODUCTS AND FIRE INTENSITY

Previous measurements by Pereira *et al.* (1996a) have shown that there is a good positive correlation between the amount of aerosol particles on a vertical column of the atmosphere, measured by using an instrumented airplane, and the number of fire spots counted in a region around the site where these measurements were performed. This region will be henceforth referred to as circle of investigation. Data for CO, CH_4 and N_2O (Volker Kirchhoff, from INPE, S.J.Campos, Brazil, pers. comm.) obtained for the same region also exhibits this behavior although with a much smaller degree of correlation with the fire spots. Table 1 shows the correlation coefficients found between these atmospheric constituents and the number of fire spots detected by satellite within a circle of investigation with 2.5° radius around the site were the vertical concentration profiles were performed. Other circles of investigations were also tested but the 2.5° radius yields the best overall correlation for all components.

All six atmospheric components increase as the fire activity in the area increases, which suggests a possible explanation for systematic deviations of the model estimations. The deviations can be

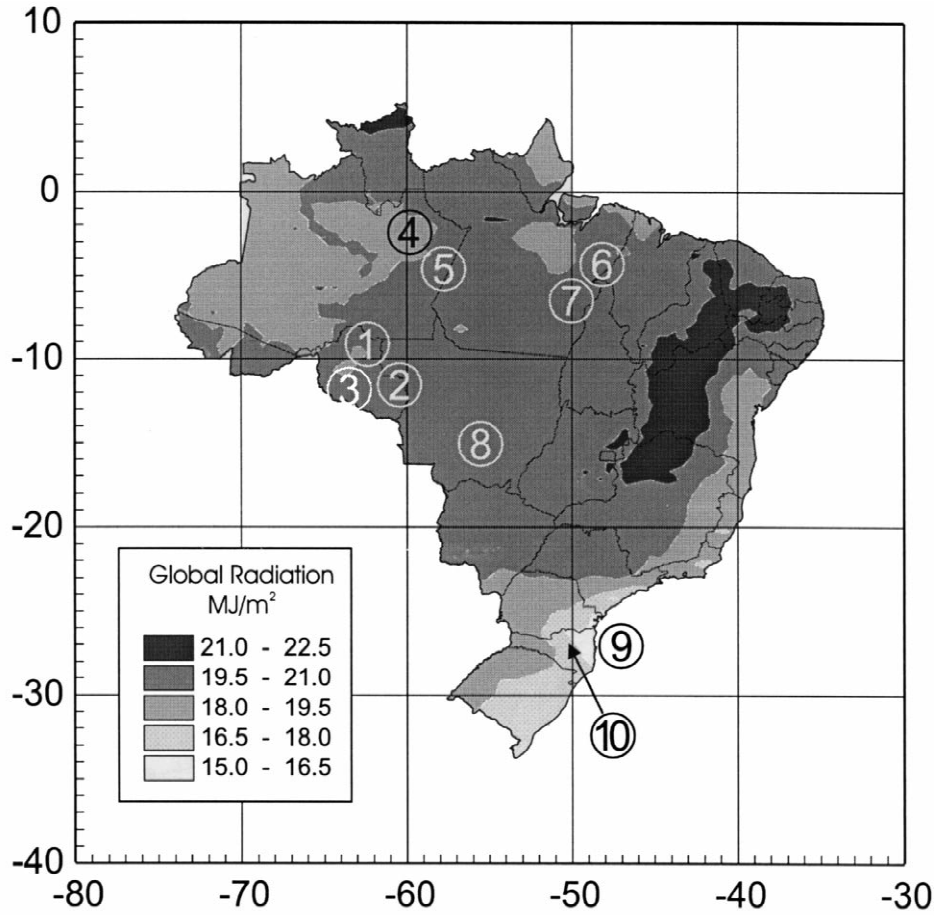

Fig. 4. Distribution of the mean horizontal global solar irradiation in Brazil estimated by the BRASIL-SR model. Values represent the daily totals averaged between 1995 and 1998. The circled figures are the approximate locations of the ground stations listed in Table 2.

linked to the injection of an additional load of particulate and gaseous fire products to the atmosphere that are not accounted for by the monthly mean climatology used as input for the BRASIL-SR model.

4.1. Ground radiation data

Available ground sites for solar radiation measurements consisted of pyranometers installed in eight sites of the Central and Amazon area of Brazil, listed in the Table 2. Two additional sites located in the southern part of Brazil were also included for comparison with results in areas free of forest fires—they are the BSRN (Baseline Surface Radiation Network, WMO) site in Florianópolis and the site at Lebon Regis, both in the state of Santa Catarina. Radiometer data for the ground sites at Potosi Mine and Cuiabá was kindly provided by Thomas F. Eck from the NASA/GSFC, Greenbelt, MD (pers. comm.) and are linked to the SCAR-B experiment. The SCAR-B (Smoke, Clouds and Radiation, Brazil) was a joint INPE-NASA/GTE experiment performed during 1995 that aimed at an evaluation of the aerosol forcing on climate due to the forest fires in Brazil. Sites of Jarú, Aparecida, Dimona, Ducke, Boa Sorte, and Rio Doce were provided by the Anglo-Brazilian Climate Observation Study (ABRACOS) project. The ABRACOS aimed at monitoring Amazonian climate, improving the knowledge of the consequences of deforestation and providing data for the calibration and validation of global circulation models and sub-models of Amazonian forest and post-deforestation pasture. Stations 4 and 5 in Table 2 are located in the middle of the Amazon tropical humid forest. Stations 1, 2, 3, 6 and 7 are located in the areas of rapid deforestation activities. Station number 8 is located in the Brazilian central plateau, in a typical area of 'Cerrados'

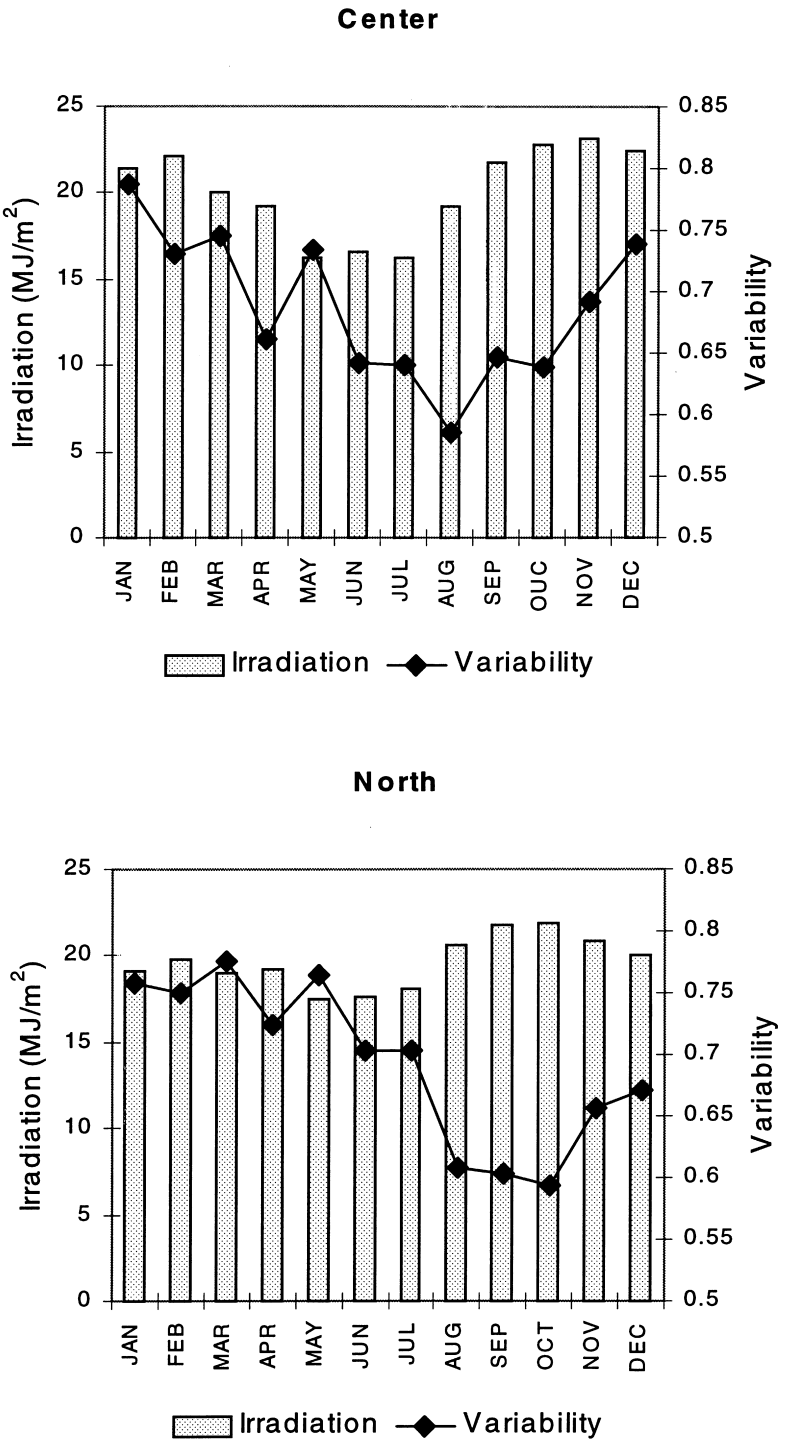

Fig. 5. Monthly variability of solar irradiation measured for the period between 1996 and 1997 for the northern and central regions of Brazil, where fires are frequent. The lines indicate the variability and the dashed columns indicate the monthly solar irradiation. The variability was calculated as the standard deviation of the daily solar irradiation divided by its mean value, for each month in all pixels of the image.

(Brazilian grassland). Stations 9 and 10 are located outside the biomass-burning region (see Fig. 4).

The first step in the ground data handling was the careful selection of clear-sky days. This was necessary since the study contemplates the

Table 1. Correlation coefficients between fire spots and fire products injected in the atmosphere

Combustion product	Correlation coefficient (R^2)	No. of profiles
Total aerosol mass	+0.98[a]	5
Black carbon	+0.97	9
Submicron particle count number	+0.95	5
CH_4	+0.90	5
N_2O	+0.65	5
CO	+0.45	5

[a] +, indicates a positive correlation.

evaluation of the effects on the satellite estimations that are caused solely by changes in the atmosphere by the fires. This choice excludes the random fluctuations on the solar radiation data caused by clouds, which is of no concern in this study. The selection of clear-sky days was made by following the procedure below:

1. For sites where both global and diffuse radiation data were available we employed a criterion based on the Liu and Jordan (Iqbal, 1983) and Aguiar and Collares-Pereira (1992) clearness index. Thus, clear days were selected when $K_t = H/H_0 > 0.6$, and the visual inspection through the curves of $K_d = H_d/H$ suggested the absence of clouds (low values of K_d). H_d is the daily diffuse solar irradiation, H is the daily global solar irradiation, and H_0 is the daily extraterrestrial solar irradiation.
2. When the diffuse solar irradiation data were not available, the procedure was less objective since we had to rely on the information provided by the K_t index alone.
3. For all sites we also inspected the time plots for the global solar irradiation raw data to spot clouds by looking at the shape and smoothness of the plots.
4. Finally, after selecting the candidates for clear-sky days using the above procedure, we visually inspected the GOES-8 satellite images at each of the ground validation sites to pick up clouds.

By using the above procedure it was possible to select a total of 235 clear-sky days for the period between March and October which comprises not only the dry season of interest for this research but also part of the rain season for comparison purposes. The number of selected measurements is different at each validation site. Some of the sites, as the BSRN station at Florianópolis with 121 clear-sky days, had a much larger number of selected data sets compared to others. Sites 4 and 5, located inside the humid tropical forest, did not present enough clear-sky days to provide valuable time information for this study.

The deviations were measured by the relative mean bias (MBE) and the relative root mean square (RMSE) errors between model estimations and ground pyranometer data, calculated by the expressions below:

$$\mathrm{MBE}(\%) = \frac{100}{\langle x_i \rangle} \times \frac{\sum_i (y_i - x_i)}{n} \tag{9}$$

$$\mathrm{RMSE}(\%) = \frac{100}{\langle x_i \rangle} \times \left(\frac{\sum_i (y_i - x_i)^2}{n} \right)^{1/2} \tag{10}$$

Where y_i and x_i are the ith model estimated and ground measured solar irradiation, respectively, n is the total number of data points and $\langle x_i \rangle$ is the average for $x_i = 1, 2, \ldots, n$.

The clear-sky deviations MBE and RMSE between model estimations and ground data are presented by the histograms in Fig. 6 along with the correlation coefficients. The plots are shown divided into two subsets: one consisting of all sites located in the region where biomass burning activities are dominant (sites 1–8), and the other for sites outside this region (sites 9 and 10). Also plotted for comparison are the deviations ob-

Table 2. Ground solar radiation stations employed for the model validation

	Site name	Location	Latitude	Longitude	Altitude (m)
1	Potosi Mine	Rondônia	9.78°S	62.87°W	80
2	Jarú forest reservation	Rondônia	10.08°S	61.92°W	120
3	N.S. Aparecida farm	Rondônia	10.75°S	62.87°W	220
4	Dimona farm	Amazonas	2.32°S	60.32°W	120
5	Ducke forest reservation	Amazonas	2.57°S	59.95°W	80
6	Boa Sorte farm	Pará	5.17°S	48.75°W	170
7	Vale do Rio Doce forest reservation	Pará	5.75°S	49.17°W	150
8	Cuiabá	Mato Grosso	15.33°S	56.07°W	152
9	Florianópolis (BSRN)	Santa Catarina	27.60°S	48.57°W	15
10	Lebon Regis	Santa Catarina	26.98°S	50.71°W	1036

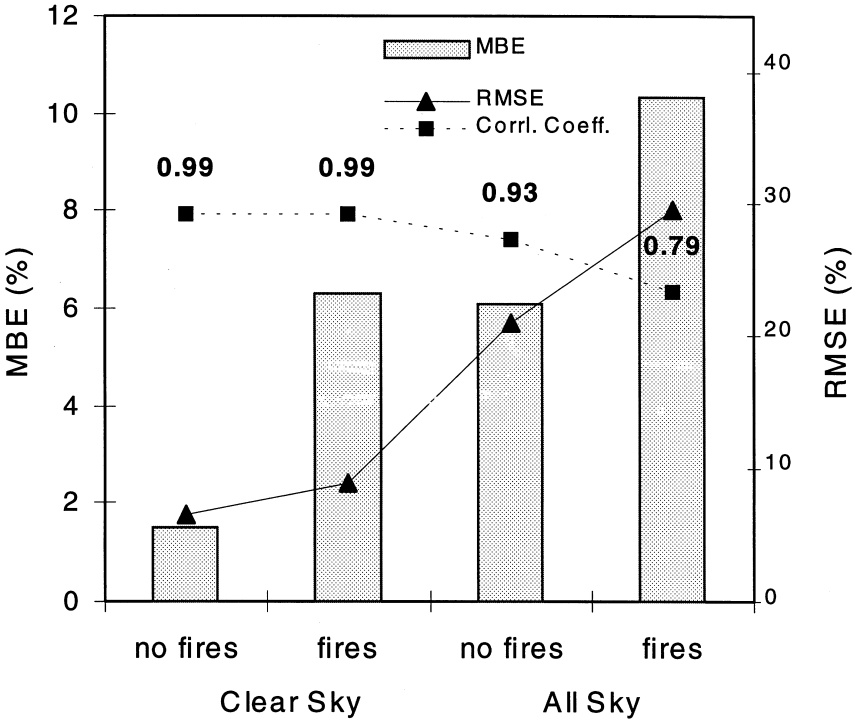

Fig. 6. Variation of systematic errors (MBE) and random errors (RMSE) between daily sums of ground data and model estimations split into two categories—for sites within and outside the biomass burning area.

served for the all-sky radiation data of these same sites.

Comparison between these two sky conditions is, however, very ambiguous because of the inclusion of the deviations caused by clouds which are, of course, dominant. The biases are consistently larger for the sites within the region of fires. The RMSE are correspondingly higher in this case. Furthermore, the correlation coefficients between measured and estimated values are larger for sites located outside the biomass burning area in the case of all-sky condition, which translates into a more consistent data set for these sites.

The annual-base clear-sky deviations for each individual validation site are shown in Table 3. For the sites located in the southern part of the country, thus outside the biomass burning area (sites 9 and 10), the RMSE's are all below 5% and the MBE's are below 1.2%. Deviations are comparatively larger for the sites located in areas of intensive burning of biomass (1–8).

The available radiation data sets for the sites at Potosi Mine and Cuiabá were very meager, which allowed the selection of only one clear-sky day each for this study, following the procedure explained above. Notwithstanding, these two sites presented the largest deviations when compared to all the other sites and days. Potosi Mine data were collected during the month of September and presented an MBE of 44%, while Cuiabá's where

Table 3. Clear-sky model validation performed on a daily basis (figures are the relative Root Mean Square Error (RMSE), relative Mean Bias Error (MBE), and the total number of clear-sky days used in this computation)

Ground site	RMSE (%)	MBE (%)	No. of days
Potosi Mine	* [a]	43.6	1
Jarú forest reservation	8.5	5.8	53
N.S. Aparecida farm	8.4	7.4	28
Dimona farm	*	*	0
Ducke forest reservation	*	9.3	1
Boa Sorte farm	6.6	6.4	8
Vale do Rio Doce forest reservation	7.2	6.4	14
Cuiabá	*	17.1	1
Florianópolis (BSRN)	4.9	1.2	121
Lebon Regis	2.8	−0.4	8
All sites	7.7	2.4	235

[a] *, Not enough data to carry on the calculation.

collected in August (MBE = 17%), the peak of the burning season. The possibility of instrumental bias is highly improbable for these sites. Measurements were taken by using Eppley PSP pyranometers during the SCAR-B mission. The calibration accuracy claimed by Eppley Laboratories is about 1%. These two pyranometers were intercalibrated and agreed with each other within 1.3%. Furthermore, the aerosol optical depth reported at these sites (Tom Eck, pers. comm.) were very high in Potosi Mine: 2.68 (340 nm), 1.75 (498 nm), 2.11 (669 nm), 1.01 (871 nm) and 0.4 (1021 nm). These values were correspondingly smaller in Cuiabá. Thus, although there is only a single clear-sky day at each of these sites, the measurements reported here are reliable.

The relative MBE and the RMSE for all ground sites located within the biomass-burning region varies with the time of the year as shown in Fig. 7. The deviations were calculated for all available clear-sky days on a daily basis. Both the MBE and the RMSE follow each other very closely which can be explained by the prevailing systematic nature of the deviations. The deviations increase between August and October in agreement with the months of maximum development of fires in the north of Brazil, as seen in Fig. 2.

Fig. 8 exhibits the plots of the variations of the calculated and measured transmittances vs. solar zenith angles for six cases: Potosi Mine, Cuiabá, Boa Sorte farm, N.S. Aparecida farm, Jarú forest reservation, and Florianópolis. These sites and days were shown here as case studies only, in order to illustrate the local impact of fire activities on the light transmittance through the atmosphere in different situations. They do not represent a particular tendency or pattern of deviation at each site and time of the year. Actually, the impact of fires on the clear-sky transmittance at each particular site is highly variable and depends not only on the fire intensity prevailing during the data collection period but also on several other parameters such as wind, the start and duration of fires, and emission factors of the local biomass, which are not available for this study. In spite of this, the examples are useful to better understand the time dependency of the fire influence on the light transmission during a day cycle.

The event of Potosi Mine, in the state of Rondônia, presents a large difference between measured and estimated light transmittance for all zenith angles, suggesting a long-term impact of fire on the atmospheric transparency. The event of Cuiabá, located in the central 'Cerrados' region of Brazil, also shows a rather large deviation that started to increase drastically from mid-morning

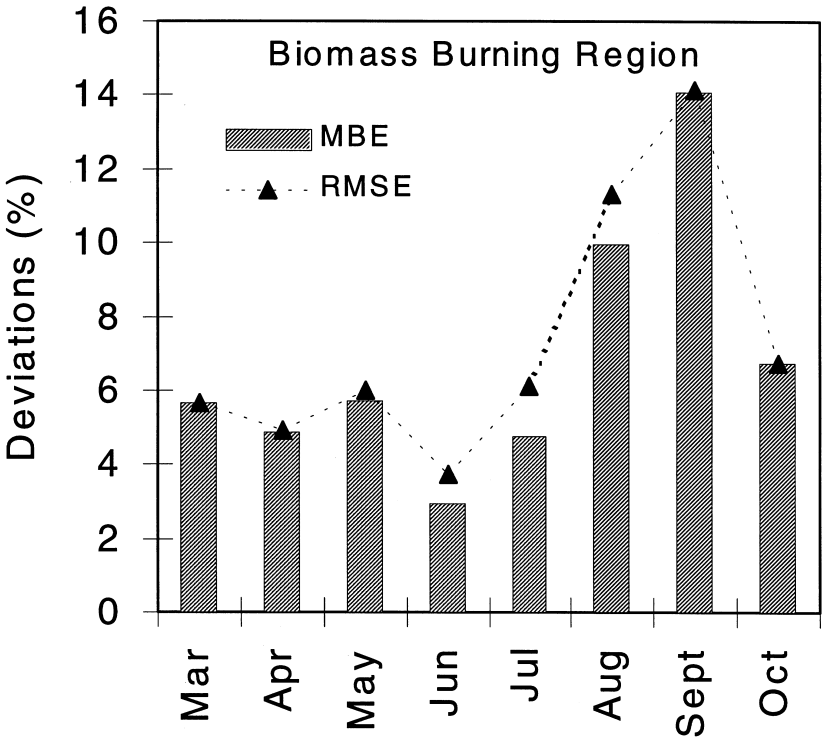

Fig. 7. Monthly variation of the daily basis MBE and RMSE calculated between ground data and satellite estimations of clear-sky solar irradiation for sites located in the biomass burning region (sites 1–8 in Table 2).

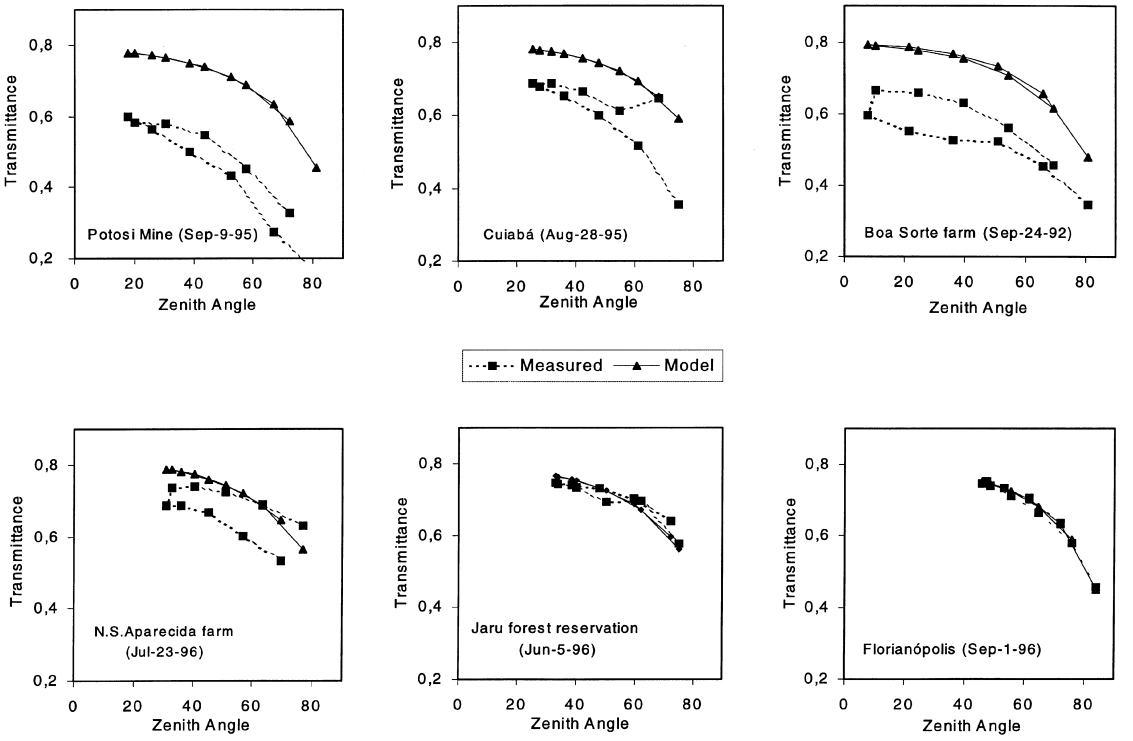

Fig. 8. Impact of fire activity on light transmittance vs. solar zenith angle for several cases.

hours. The site at Boa Sorte farm (Pará) illustrates a day with a large impact from the fires and a clear tendency to increase at about noontime and in the early afternoon hours. N.S. Aparecida farm (Rondônia) presented a distinct pattern when compared to the previous examples. This former case displays a more reduced fire influence which probably started in the mid-morning or early afternoon hours. The example of Jarú forest reservation (Rondônia) represents a condition of little deviation encountered more often outside the burning season for this region (see Fig. 7). Finally, the site at Florianópolis (Santa Catarina) is an example of the result found in a region not usually subjected to the impact of biomass burning and, thus, displays a good fit between the two curves for all solar zenith angles.

4.2. Fire dependency of systematic errors

The MBE for sites located within the areas of burning of biomass (Aparecida, Boa Sorte, Cuiabá, Duke, Jarú, Potosi, and Rio Doce) are dependent on the time of year. The maximum bias is found for the month of September when the fire activities in this area is also at its maximum. Fig. 9 depicts the time behavior of the measured MBE for all stations, along with the monthly relative frequency of fire spots in this selected region as a function of the time of the year. The agreement between the two curves suggests that these two variables are linked to each other.

This observation is supported by the cross-correlation analyses [Fig. 10(a)] performed between time series for the fire spots counted over the five major climatic regions of Brazil and the relative systematic error MBE for all sites 1–8 in Table 2. The best agreement is found for zero lag in the North region. The maximum correlation is in phase with the dry season. During this period, the model has the strongest tendency to overesti-

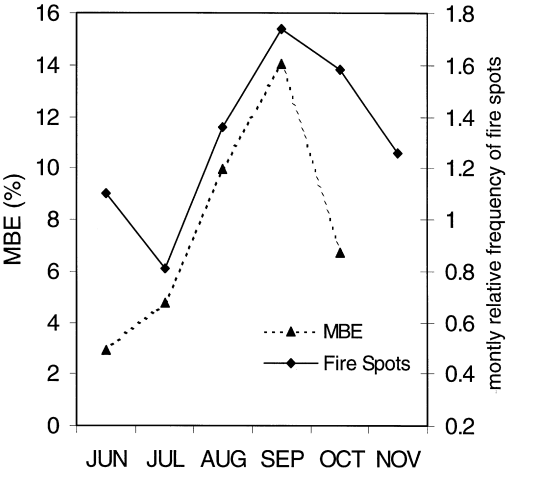

Fig. 9. Time series for the MBE and the relative increment of fire spots in areas of intensive burning of biomass.

mate the incoming global surface irradiation. This can be attributed to the large amounts of aerosols injected into the atmosphere that are not accounted for by the simple climatology used in the BRASIL-SR model.

For the Central region some correlation is also shown, but with a 1–2-month time lag. This is explained by the fact that the peak of the burning season in this area occurs 1–2 months before this peak in the northern region. Vegetation in this area is mostly 'Cerrado' which has an intrinsic lower emission power when compared to the forest up in the northern region. Furthermore, the general atmospheric circulation in Brazil, which is ruled by the tropical Atlantic high-pressure center, sets the prevailing low-level winds from the sector North–Northeast. Thus the region probably introduces only a minor contribution to the observed biases.

For comparison purposes, the same cross-correlation study was made [Fig. 10(b)] for the validation site at Florianópolis, which is located in a region where biomass burning is very low all year round. The zero lag correlation was observed between the regional fire spots and the observed biases for the South. This indicates that regional fires, although negligible, may produce some local effects in the sunlight transmittance. A better zero lag time correlation was obtained between fire spots counted in the northern region and the MBE. This is evidence for the outflow of biomass burning products to the Atlantic Ocean pointed out by several authors (Pereira *et al.*, 1996b; Anderson *et al.*, 1996)

The plot of the bias between the irradiance measured by ground stations and model estimations vs. the fire spot counts is shown in Fig. 11. Fire counts are shown on a logarithmic scale to account for the order of magnitude changes observed for this parameter. Indeed, this is only a crude evaluation for the cause–effect relationship between these two variables. The large scattering of data may be attributed to variable meteorological conditions prevailing at each of the observations, superimposed on the effects of several stages of biomass burning (flaming or smoldering) and on the different emission factors found at each particular site. Thus, depending on the prevailing winds with respect to the fire spots, we may have different situations where the fire spot concentrations are downwind or upwind, thus affecting the net results which is based on a 2.5° circle of investigation in this study. However, this dispersion in the data points does not conceal the positive correlation between the bias and the fire spots, there is a 95% confidence level.

5. CONCLUSIONS

Forest fires are responsible for the injection of a variable amount of aerosols and optically active gases into the atmosphere. This may account for a corresponding attenuation in the solar radiation flux at the surface. This work has shown a positive correlation between the fire spots counted using the satellite technique and the vertical column concentration of some of these fire products (aerosols, black carbon, N_2O, CO and CH_4). This correlation suggests a possible tool to help the parameterization of the effects of the aerosols on radiation transfer models.

Observed systematic deviations between ground measurements and satellite estimations are larger in areas where intensive burning of biomass is the practice for land clearings for farming and cattle growth. This is true not only for clear-sky days but also for all sky days. For clear-sky days, the MBE is about four times larger in sites located within the burning areas while for the all sky days this factor is less than two. The RMSE is low for the clear-sky days in regions without burning compared to the RMSE obtained for the all sky conditions. This is explained by the superimposed effect of clouds in the last case. Thus, the effects of clouds apparently do not conceal the bias originated by the contribution of the forest fires.

The combustion products injected into the atmosphere during the fire season (July–October) in Brazil may explain part of the systematic deviations found between the BRASIL-SR radiation model estimations and ground radiation data from pyranometers. The time series of monthly MBE measured for sites located in the region of burning in Fig. 7 for clear-sky days show an increase of 3–4 times during the fire season when compared to the data available for the rest of the year. Stations located in the southern part of the country presented very low MBE (−0.4% and 1.2%). These stations are located outside the region of intensive burning of biomass.

The satellite-counted fire spots are well correlated with the observed MBE between the satellite estimations and the ground data. This is clear for the time series of these two variables in sites located within the area of intensive biomass burning. Both presented a peak value around the month of September, when the combined MBE for all stations reached about 14%. A cross-correlation study performed by comparing the time series of fire spots and the MBE support this conclusion for the northern region of the country.

The same cross-correlation study was also made for a site (Florianópolis) far outside the

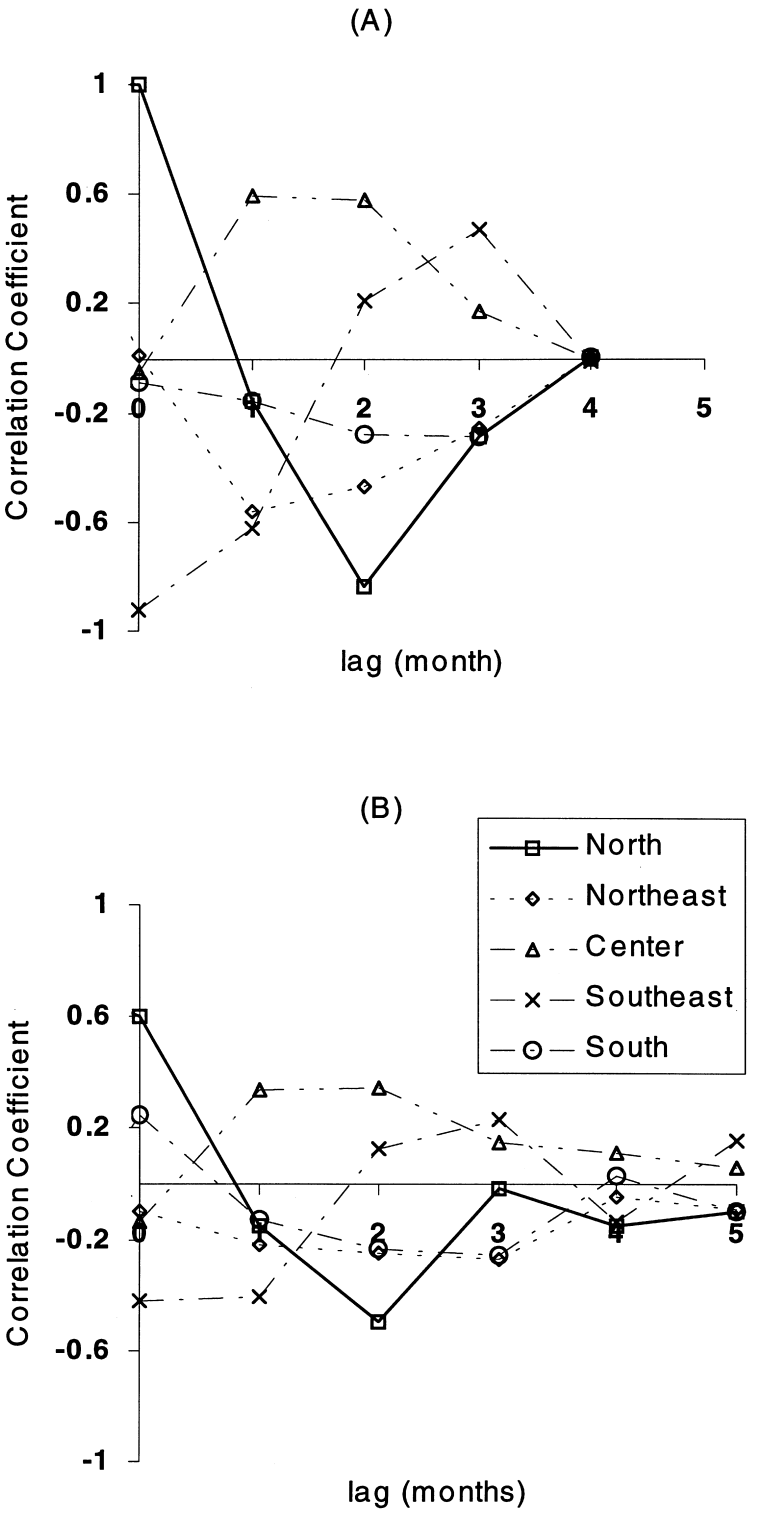

Fig. 10. Cross-correlation between time series for MBE and fire spots performed for validation sites located in the biomass burning area (a), and for the site outside this area, in Florianópolis (b).

major areas of burning biomass in Brazil. Although the influence of the local fires is very reduced in this case, it is still clearly discernible. Furthermore, this study has shown that fires in the northern region are responsible for an increase in the MBE in the South, by the atmospheric transport of combustion products. The driving mechanism for this transport is the mesoscale atmospheric circulation pattern linked to the outflow of these products to the Atlantic Ocean.

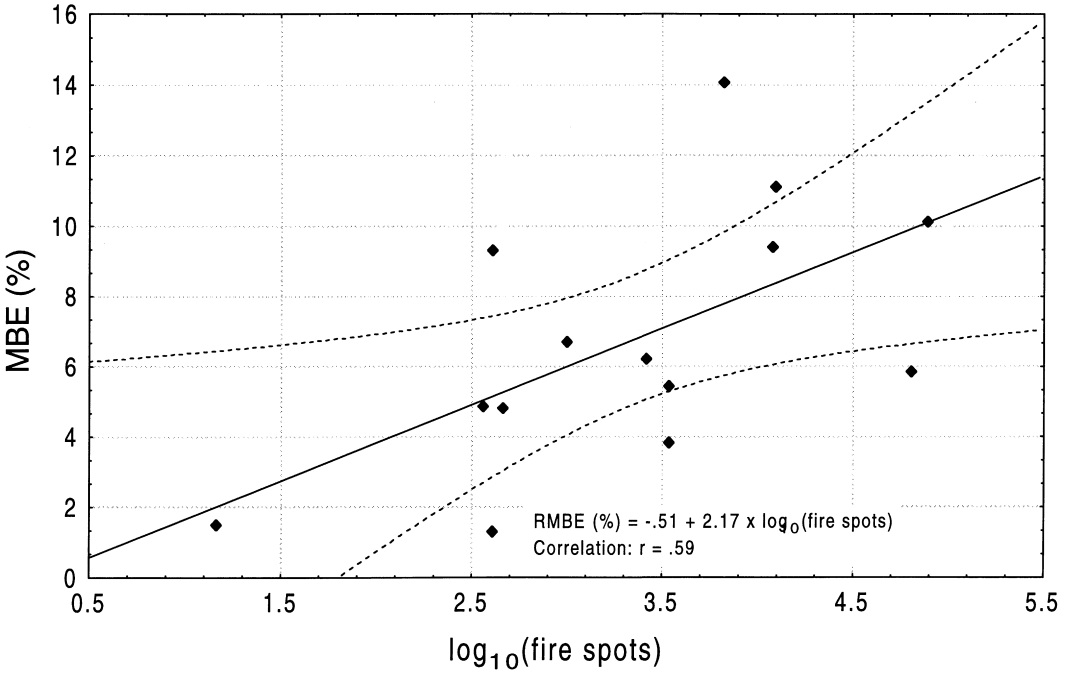

Fig. 11. Plot of the relative mean bias error (MBE) and the logarithm of the number of fire spots counted inside a 2.5° circle of investigation around the ground solar station. The dotted line represents the 95% confidence level for the straight-line fitting.

This study is the first step in an effort to derive a routine procedure to be included in the BRASIL-SR radiation model, in order to adequately parameterize the variable effect of the forest fires in Brazil. In order to conform this procedure to the routine operation of the model, it must rely on some available direct or indirect information on the amount and variation of the combustion products in the atmosphere. Thus the possibility of employing the fire spot counts for this purpose is encouraging.

Acknowledgements—Thanks are due to the following colleagues: Carlos Nobre, Alberto W. Setzer, Sérgio Pereira, Mateus A.R. Andrade, Marcos C. Pereira, Volker W.J.H. Kirchhoff, and Thomas F. Eck. The following institutional acknowledgement is also due: the Center for Weather Forecasts and Climatic Studies, CPTEC/INPE. This work was supported by a grant from FAPESP (No. 96/1243-7).

REFERENCES

Aguiar R. J. and Collares-Pereira M. (1992) Statistical properties of hourly global radiation. *Solar Energy* **48**, 157–167.

Anderson B. E., Grant W. B., Gregory G. L., Browell E. V., Collins Jr. J. E., Sachse W. G., Bagwell D. R., Hudgins C. H., Blake D. R. and Blake N. J. (1996) Aerosols from burning over the tropical South Atlantic region: Distributions and impacts. *J. Geophys. Res.* **101**(24), 117–137.

Charlson R. J., Schwartz S. E., Hales J. M., Cess R. D., Coakley Jr. J. A., Hansen J. E. and Hofmann D. J. (1992) Climate forcing by antropogenic aerosols. *Science* **255**, 423–430.

Coakley J. A., Cess R. D. and Yurevich F. B. (1993) The effect of tropospheric aerosols on the Earth's radiation budget: A parameterization for climate models. *J. Atmos. Sci.* **40**(1), 116–138.

Crutzen P. J. and Andreae M. O. (1990) Biomass burning in the tropics: Impact on atmospheric chemistry and biogechemical cycles. *Science* **250**, 1669–1677.

Ferek R. J., Reid J. S., Hobbs P. V., Blake D. R. and Liousse C. (1997) Emission factors of hydrocarbons, halocarbons, trace gases and particles from biomass burning in Brazil. *Proceedings of the SCAR-B Meeting,* in Fortaleza, November, 1996, pp. 43–54, Transtec Editorial.

INMET (1992) *Normais Climatológicas (1961–1990),* 84 p., Ministério da Agricultura – Instituto Nacional de Meteorologia, Brazil.

Iqbal M. (1983). In *An Introduction to Solar Radiation*, p. 390, Academic Press, Toronto, Canada.

Kirchhoff V. W. J. H. (Ed.) (1996) *SCAR-B Proceedings*, 207 p., São José dos Campos: Transtec Editorial, Collection of papers presented at the Fortaleza, Brazil, workshop.

Lenoble J. (1985). In *Radiative transfer in scattering and absorbing atmospheres: Standard computational procedures*, A. Deepak Publishing, Hampton, 420 p.

McClatchey R. A. and Selby J. E. (1972) *Atmospheric Transmittance from 0.25 to 38.5 μm: Computer Code LOWTRAN-2,* Air Force Cambridge Research Lab., AFCRL-72-0745, Environ. Res. Paper 427.

Möser W. and Raschke E. (1983) Mapping of global radiation and of cloudiness from Meteosat image data. *Meteorol. Rdsch.* **36**, 33–41.

Pereira E. B., Abreu S. L., Stuhlmann R., Rieland M. and Colle S. (1996a) Survey of the incident solar radiation in Brazil by use of Meteosat satellite data. *Solar Energy* **57**(2), 125–132.

Pereira E. B., Setzer A. W., Gerab F., Artaxo P. E., Pereira M. C. and Monroe G. (1996b) Airborne measurements of burning of biomass aerosols in Brazil related to TRACE-A experiment. *J. Geophys. Res.* **101**(D19), 23983–23992.

Pereira M. C. and Setzer A. W. (1993) Spectral characteristics of deforestation fires in NOAA/AVHRR images. *Int. J. Remote Sens.* **14**(3), 583–597.

Schmetz J. (1984) On the parameterization of the radiative properties of broken clouds. *Tellus* **36**, 417–432.

Ward D. E., Sussot R. A., Kauffman J. B., Babbitt R. E., Cummings D. L., Dias B., Holben B. N., Kaufman Y. J., Rasmussen R. A. and Setzer A. W. (1992) Smoke and fire characteristics for cerrado and deforestation burns in Brazil: BASE-B experiment. *J.Geophys. Res.* **97**, 14601–14619.

Whitlock C. H. and Tarplay D. (1996) Satellite-based solar radiation data archives and new data, *Proceedings of the Workshop: Satellites for Solar Energy Resource Information*, April 10–11, 1996, Washington, DC.